Image potentials and an inverse dielectric response function for a semiconductor slab

Ami C. Sharma*
Cavendish Laboratory, University of Cambridge, Madingley Road, Cambridge CB3 OHE, United Kingdom
(Received 10 July 1985; revised manuscript received 28 February 1986)

We report an inverse random-phase-approximation dielectric response function $\epsilon^{-1}(\mathbf{r},\mathbf{r}',\omega)$ within an extreme tight-binding model for a semiconductor slab of any thickness d. With the use of $\epsilon^{-1}(\mathbf{r},\mathbf{r}',\omega)$ the image potentials for a charged particle have been calculated in the long-range interaction limit for various possible cases.

I. INTRODUCTION

There is a great deal of interest in the properties of a semiconductor slab from the standpoints of both technology and physics. The dielectric response function of any system provides considerable information about the system. A number of properties such as the image potentials, the response of a system to varying external fields, the screened impurity potential, collective excitations, energy loss of charged particles, optical properties, self-energies, and the phonon spectrum can be studied by knowing the dielectric response function.[1–16] During recent years, calculations have been done for a dielectric function $\epsilon(\mathbf{q},\omega)$ for a semiconductor slab.[17,18] However, unfortunately, most of the above-mentioned properties depend on an inverse dielectric response function. Obtaining the inverse dielectric response function is a major problem, even for a perfect crystal. In principle, it involves an infinite matrix. In the case of a slab, additional complications are introduced by the finite geometry of the slab, which reduces the crystal symmetry. In an earlier communication, we showed that $\epsilon(\mathbf{q},\omega)$ of a slab has a more complicated form than that of a semi-infinite or infinite solid, even in $\mathbf{q}\rightarrow\mathbf{0}$ limit.[17–22]

Other classical or semiclassical methods have been used to study the surface excitations and the image potentials in a slab.[19] These methods borrow from classical electrodynamics and the bulk response function and are based on various matching conditions. Using these methods, one can obtain a reasonable solution of the problem, but since these methods involve large numbers of quantities, they sometimes appear quite confusing and unphysical. Thus, it seems worthwhile to develop an alternative approach, i.e., to develop an inverse dielectric response formula based on well-known physical and mathematical concepts starting from a microscopic treatment.

In the past, significant progress was made in obtaining an inverse dielectric response function for the perfect crystal in certain approximations.[1,7,9,11–13,23–29] It has been shown that an inverse dielectric response function for a perfect crystal can be obtained in both Fourier space and real space, even including local-field effects and excitonic effects, for example, because of the complete crystal symmetry. Sinha *et al.*[29] obtained an inverse dielectric response function in Fourier space by making a general ansatz for the form of the dielectric response function. The various existing models for dielectric matrix can be derived from the work of Sinha *et al.* for different kinds of perfect solids. For systems with finite geometry and crystal defects, the real-space formulation has major advantages. Keeping this in mind, we calculate an inverse random-phase-approximation (RPA) dielectric response function in real space, $\epsilon^{-1}(\mathbf{r},\mathbf{r}',\omega)$, for a semiconductor slab.

Although the detailed numerical calculation of $\epsilon^{-1}(\mathbf{r},\mathbf{r}',\omega)$ has many advantages, its use for other investigations is very difficult. Thus, for practical applications, one requires a conceptually convincing and simple formulation. In view of this, we report in this article a compact form of $\epsilon^{-1}(\mathbf{r},\mathbf{r}',\omega)$ for a semiconductor slab, using the extreme tight-binding (ETB) model. With the use of $\epsilon^{-1}(\mathbf{r},\mathbf{r}',\omega)$, we then calculate the image potentials of a charged particle for various possible cases in the long-range interaction limit. The potential usefulness of tight-binding approximations for semiconductors and insulators have been demonstrated by Sinha.[30] Further extension of our calculation beyond the ETB model, in order to obtain more detailed information, can be done easily. This will be done in forthcoming work. The main aim of this article is to show that a unifying approach, successfully used for perfect crystals, can also be used for more complicated systems with lower symmetry. Also, our calculations suggest that this method can be easily applied for small clusters and heterostructures. The outline of our article is as follows: In Sec. II, we report the calculation of $\epsilon^{-1}(\mathbf{r},\mathbf{r}',\omega)$. The image potentials of a charged particle are reported in Sec. III. We discuss and conclude our results in Sec. IV.

II. INVERSE DIELECTRIC RESPONSE FUNCTION

Within the ETB model, the real part of the inverse RPA dielectric response function is given by[28]

$$\epsilon^{-1}(\mathbf{r},\mathbf{r}',\omega)=\delta(\mathbf{r}-\mathbf{r}')+N_0(\omega)\times\sum_{\substack{\nu,\nu'\\ \mathbf{R},\mathbf{R}'}}\int d^3r''\,v(\mathbf{r}-\mathbf{r}'')A_\nu(\mathbf{r}-\mathbf{R})\times\left[Q^{\nu\nu'}_{\mathbf{R}\mathbf{R}'}\right]^{-1}A_{\nu'}(\mathbf{r}'-\mathbf{R}') \quad (1)$$

with

$$Q^{\nu\nu'}_{\mathbf{R}\mathbf{R}'}=\delta^{\nu\nu'}_{\mathbf{R}\mathbf{R}'}-N_0(\omega)\int\int d^3\lambda\, d^3\rho\, A_\nu(\boldsymbol{\lambda}-\mathbf{R})v(\boldsymbol{\lambda}-\boldsymbol{\rho})\times A_{\nu'}(\boldsymbol{\rho}-\mathbf{R}'), \tag{2}$$

where

$$N_0(\omega)=-4E_g/(E_g^2-\hbar^2\omega^2) \tag{3}$$

and

$$A_\nu(\boldsymbol{\lambda}-\mathbf{R})=\phi^v_\nu(\boldsymbol{\lambda}-\mathbf{R})\phi^c_\nu(\boldsymbol{\lambda}-\mathbf{R}) . \tag{4}$$

In these equations, E_g is the energy band-gap parameter, $v(\mathbf{r}-\mathbf{r}')$ is the Coulomb potential, and $\Phi^v_\nu(\mathbf{r}-\mathbf{R})\Phi^c_\nu(\boldsymbol{\lambda}-\mathbf{R})$ are the localized valence- and conduction-band orbitals at atomic site $\mathbf{R}$ with orientation index ν. The other symbols have their usual meaning.

The physical basis of this model is that the system is composed of polarizable bonds. Each bond is characterized by bonding and antibonding orbitals separated by constant energy E_g. Application of an external perturbation polarizes the bonds. These bonds interact self-consistently through multipole-multipole (in the long-range interaction limit, dipole-dipole) interactions. These interactions are included in $(Q^{\nu\nu'}_{\mathbf{R}\mathbf{R}'})^{-1}$.

The inversion of $\epsilon(\mathbf{r},\mathbf{r}',\omega)$ depends on the inversion of the matrix $Q^{\nu\nu'}_{\mathbf{R}\mathbf{R}'}$; let us write

$$\underline{Q}^{-1}=(1-N_0\underline{C})^{-1}=1+N_0\underline{C}+N_0^2\underline{C}\,\underline{C}+N_0^3\underline{C}\,\underline{C}\,\underline{C}+\cdots , \tag{5}$$

where

$$\underline{C}=\int\int d^3\lambda\, d^3\rho\, A_\nu(\boldsymbol{\lambda}-\mathbf{R})v(\boldsymbol{\lambda}-\boldsymbol{\rho})A_{\nu'}(\boldsymbol{\rho}-\mathbf{R}') . \tag{6}$$

Thus, $\underline{Q}^{-1}$ is a sum of the terms involving the matrix products. The series given by Eq. (5) is a converging series, as we will see later on. Let us consider the matrix product

$$\underline{C}\,\underline{C}=\sum_{\nu'',\mathbf{R}''}\int\int d^3\lambda\, d^3\rho\, A_\nu(\boldsymbol{\lambda}-\boldsymbol{\rho})v(\boldsymbol{\lambda}-\boldsymbol{\sigma})A_{\nu''}(\boldsymbol{\sigma}-\mathbf{R}'')\times\int\int d^3\sigma\, d^3\rho\, A_{\nu'}(\boldsymbol{\sigma}-\mathbf{R}'')v(\boldsymbol{\sigma}-\boldsymbol{\rho})\times A_{\nu'}(\boldsymbol{\rho}-\mathbf{R}') . \tag{7}$$

$\underline{C}$ involves both long-range as well as short-range interactions. The internal summations in $\underline{C}\,\underline{C}$ are averaged over the volume of the slab, and long-range interactions make a dominant contribution, since they fall off slowly. Thus, in order to make the calculation simple and to obtain practically applicable results, one can safely ignore the short-range effects. In the long-range interaction limit, $\underline{C}$ reduces to a dipole-dipole interaction matrix, and $\underline{C}\,\underline{C}$ can be written as

$$\underline{C}\,\underline{C}=\sum_{\nu'',\mathbf{R}''}\{\mathbf{d}_\nu\cdot\nabla[\mathbf{d}_{\nu''}\cdot\nabla''\Phi(\mathbf{R}-\mathbf{R}'')]\}\times\{\mathbf{d}_{\nu''}\cdot\nabla''[\mathbf{d}_{\nu'}\cdot\nabla'\Phi(\mathbf{R}''-\mathbf{R}')]\}, \tag{8}$$

where

$$\mathbf{d}_\nu=e\int\boldsymbol{\rho}A_\nu(\boldsymbol{\rho})d^3\rho \tag{9}$$

and

$$\Phi(\mathbf{R}-\mathbf{R}')=1/|\mathbf{R}-\mathbf{R}'| . \tag{10}$$

Equation (8) carries summation on ν'' and $\mathbf{R}''$. For a particular $\mathbf{R}''$ sum over ν'' yields a mean-square dipole moment d^2. Thus, we have

$$\underline{C}\,\underline{C}=d^2\sum_{\mathbf{R}''}\mathbf{d}_\nu\cdot\nabla\{\nabla''\Phi(\mathbf{R}-\mathbf{R}'')\cdot\nabla''\times[\mathbf{d}_{\nu'}\cdot\nabla'\Phi(\mathbf{R}''-\mathbf{R}')]\} . \tag{11}$$

The sum on $\mathbf{R}''$ can be converted into an integration over $\mathbf{R}''$. With the use of a vector identity and the divergence theorem, Eq. (11) can be separated into two terms, one having surface integration and the other having volume integration:

$$\underline{C}\,\underline{C}=d^2n_0\,\mathbf{d}_\nu\cdot\nabla\times\left[\int d\mathbf{s}\cdot\nabla''\Phi(\mathbf{R}-\mathbf{R}'')\mathbf{d}_{\nu'}\cdot\nabla'\Phi(\mathbf{R}''-\mathbf{R}')-\int d^3R''(\nabla'')^2\Phi(\mathbf{R}-\mathbf{R}'')\mathbf{d}_{\nu'}\cdot\nabla'\Phi(\mathbf{R}''-\mathbf{R}')\right], \tag{12}$$

where n_0 is the atomic density and $d\mathbf{s}$ is the vector area along the outward normal to the surfaces. Looking at Eq. (12) we notice that as

$$(\nabla'')^2\Phi(\mathbf{R}-\mathbf{R}'')=-4\pi\delta(\mathbf{R}-\mathbf{R}'') ,$$

the second term involves pure bulk effects. This has nothing to do with finite-geometry effects. The finite-geometry effects emerge in first term. It can easily be shown that the first term is zero for an infinite geometry. We now evaluate the integrals of Eq. (12) for a dielectric slab. We define the slab as extended to infinity along the x-y plane and having finite thickness d along the z axis with boundaries at $|z|=|d/2|$, as shown in Fig. 1.

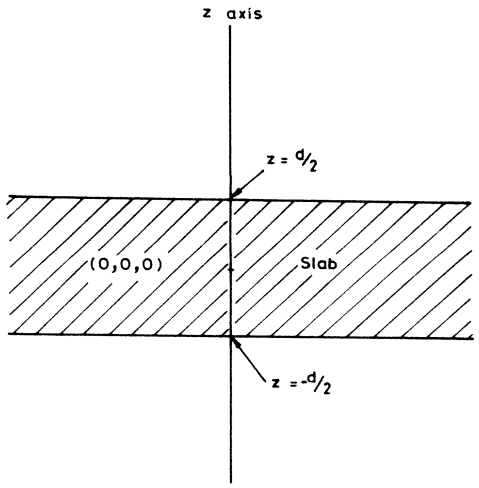

FIG. 1. Geometry of the slab.

The surface integrals in Eq. (12) can be evaluated easily by using the Fourier transforms of $\Phi(\mathbf{R}-\mathbf{R}'')$ and $\Phi(\mathbf{R}''-\mathbf{R}')$. We obtain

$$\underline{C}\,\underline{C}=\alpha(\underline{C}-\tfrac{1}{2}\underline{D}_1), \tag{13}$$

where we defined

$$\alpha=4\pi d^2 n_0 \tag{14}$$

and

$$\underline{D}_1=\mathbf{d}_\nu\cdot\nabla(\mathbf{d}_\nu\cdot\nabla'\Phi_1), \tag{15}$$

with

$$\Phi_1=1\Big/\left[(\mathbf{R}_{||}-\mathbf{R}'_{||})^2+\left[\left|R_\perp-\frac{d}{2}\right|+\left|R'_\perp-\frac{d}{2}\right|\right]^2\right]^{1/2}+1\Big/\left[(\mathbf{R}_{||}-\mathbf{R}'_{||})^2+\left[\left|R_\perp+\frac{d}{2}\right|+\left|R'_\perp+\frac{d}{2}\right|\right]^2\right]^{1/2}. \tag{16}$$

We now consider the next matrix product $\underline{C}\,\underline{C}\,\underline{C}$ in Eq. (5),

$$\underline{C}\,\underline{C}\,\underline{C}=\alpha(\underline{C}\,\underline{C}-\tfrac{1}{2}\underline{C}\,\underline{D}_1). \tag{17}$$

The new matrix product we have to evaluate is $\underline{C}\,\underline{D}_1$. Performing the calculation similar to that of $\underline{C}\,\underline{C}$, we obtain

$$\underline{C}\,\underline{D}_1=\frac{\alpha}{2}(\underline{D}_1-\underline{D}_2), \tag{18}$$

where

$$\underline{D}_2=\mathbf{d}_\nu\cdot\nabla(\mathbf{d}_\nu\cdot\nabla'\Phi_2), \tag{19}$$

with

$$\Phi_2=1\Big/\left[(\mathbf{R}_{||}-\mathbf{R}'_{||})^2+\left[\left|R_\perp+\frac{d}{2}\right|+d+\left|R'_\perp-\frac{d}{2}\right|\right]^2\right]^{1/2}+1\Big/\left[(\mathbf{R}_{||}-\mathbf{R}'_{||})^2+\left[\left|R_\perp-\frac{d}{2}\right|+d+\left|R'_\perp+\frac{d}{2}\right|\right]^2\right]^{1/2}. \tag{20}$$

In order to evaluate the next matrix product in Eq. (5), we have to calculate $\underline{C}\,\underline{D}_2$. Performing the calculation similar to that for $\underline{C}\,\underline{C}$ and $\underline{C}\,\underline{D}_1$, we obtain

$$\underline{C}\,\underline{D}_2=\frac{\alpha}{2}(\underline{D}_2-\underline{D}_3), \tag{21}$$

where $\underline{D}_3$ is defined similar to $\underline{D}_2$ with

$$\Phi_3=1\Big/\left[(\mathbf{R}_{||}-\mathbf{R}'_{||})^2+\left[\left|R_\perp-\frac{d}{2}\right|+2d+\left|R'_\perp-\frac{d}{2}\right|\right]^2\right]^{1/2}+1\Big/\left[(\mathbf{R}_{||}-\mathbf{R}'_{||})^2+\left[\left|R_\perp+\frac{d}{2}\right|+2d+\left|R'_\perp+\frac{d}{2}\right|\right]^2\right]^{1/2}. \tag{22}$$

Looking at Eqs. (15)–(25), we can generalize

$$\underline{C}\underline{D}_n=\frac{\alpha}{2}(\underline{D}_n-\underline{D}_{n+1}), \tag{23}$$

where

$$\underline{D}_n=\mathbf{d}_\nu\cdot\nabla\left[\mathbf{d}_\nu\cdot\nabla'\Phi_n\right], \tag{24}$$

with

$$\Phi_n(\mathbf{r})=1/[(\mathbf{R}_{||}-\mathbf{R}'_{||})^2+\lambda_n^2]^{1/2}+1/[(\mathbf{R}_{||}-\mathbf{R}'_{||})^2+(\lambda'_n)^2]^{1/2}, \tag{25}$$

where

$$\lambda_n=\left|R_\perp-\frac{d}{2}\right|+(n-1)d+\left|R'_\perp+(-1)^n\frac{d}{2}\right| \tag{26}$$

and

$$\lambda'_n=\left|R_\perp+\frac{d}{2}\right|+(n-1)d+\left|R'_\perp-(-1)^n\frac{d}{2}\right|. \tag{27}$$

Here, we note that $\underline{C}$ gives the dipole-dipole interaction between real dipoles while $\underline{D}_1,\underline{D}_2,\ldots,\underline{D}_n$ yield the dipole-dipole interactions between the real dipole and the image dipole. $\underline{D}_n$ involves the image of the order $_n$. Substituting the values of various matrix products in terms of $\underline{D}_1,\underline{D}_2,\ldots,\underline{D}_n,\underline{C}$, into Eq. (5), we obtain

$$\begin{aligned}\underline{Q}^{-1}=1&+N_0\underline{C}(1+N_0\alpha+N_0^2\alpha^2+\cdots)\\&-\frac{N_0^2\alpha}{2}\underline{D}_1(1+\tfrac{3}{2}N_0\alpha+\tfrac{7}{4}N_0^2\alpha^2+\cdots)\\&+\frac{N_0^3\alpha^2}{4}\underline{D}_2(1+2N_0\alpha+\tfrac{11}{4}N_0^2\alpha^2+\cdots)\\&-\frac{N_0^4\alpha^3}{8}\underline{D}_3(1+\tfrac{5}{2}N_0\alpha+\cdots)+\cdots.\end{aligned} \tag{28}$$

Summing up the various series, we obtain

$$\underline{Q}^{-1}=1+\frac{N_0(\omega)}{\epsilon(\omega)}\left[\underline{C}+\sum_{n=1}^{\infty}\left[\frac{\epsilon(\omega)-1}{\epsilon(\omega)+1}\right]^n\underline{D}_n\right], \tag{29}$$

where

$$\epsilon(\omega)=1+N_0(\omega)\alpha=1+\hbar^2\omega_p^2/(E_g^2-\hbar^2\omega^2)$$

is the "long-wavelength" bulk dielectric function. As we mentioned before, $\underline{Q}^{-1}$ includes various screened dipole-dipole interactions between real dipoles and between the real and image dipoles. One can draw a physical picture of the dipole interactions as follows; two dipoles with orientation indices ν and ν' are situated at $\mathbf{R}$ and $\mathbf{R}'$, respectively, inside the slab. These dipoles form various images from the two surfaces of slab. The real as well as image dipoles interacts self-consistently with each other via long-range interactions. It can be easily checked that Eqs. (2) and (29) satisfy the matrix property $\underline{Q}\,\underline{Q}^{-1}=1$. It is obvious from Eq. (29) that the serious expression of $\underline{Q}^{-1}$ is convergent. Substituting Eq. (29) into Eq. (1), we obtain an inverse dielectric response function for a slab:

$$\epsilon^{-1}(\mathbf{r},\mathbf{r}',\omega)=\delta(\mathbf{r}-\mathbf{r}')+N_0(\omega)\sum_{\nu,\mathbf{R}}\int d^3r''\,v(\mathbf{r}-\mathbf{r}'')A_\nu(\mathbf{r}-\mathbf{R})A_{\nu'}(\mathbf{r}'-\mathbf{R}')$$
$$+\frac{N_0^2(\omega)}{\epsilon(\omega)}\sum_{\substack{\nu,\nu'\\ \mathbf{R},\mathbf{R}'}}\int d^3r''\,v(\mathbf{r}-\mathbf{r}'')A_\nu(\mathbf{r}-\mathbf{R})A_{\nu'}(\mathbf{r}'-\mathbf{R}')\left[(C^{\nu\nu'}_{\mathbf{R}\mathbf{R}'})+\sum_{n=1}^{\infty}\left[\frac{\epsilon(\omega)-1}{\epsilon(\omega)+1}\right]^n(D^{\nu\nu'}_{n\mathbf{R}\mathbf{R}'})\right]. \tag{30}$$

On the right-hand side of Eq. (30), the second term is an on-site term while the third term and the terms under the summation are interaction terms. The second and third terms, which have been obtained before,[28] have nothing to do with the finite geometry of the slab. The finite-geometry effects emerge in the terms under summation. We should note, here, that although we have neglected the short-range interactions in obtaining $\underline{Q}^{-1}$, $\epsilon^{-1}(\mathbf{r},\mathbf{r}',\omega)$ contains a great deal of information about the short-range interactions. This information can be obtained with the use of appropriate bond orbitals in Eq. (30). In order to demonstrate a simple application of our model $\epsilon^{-1}(\mathbf{r},\mathbf{r}',\omega)$, we calculate the image potentials of a point charge using Eq. (29) in the long-range interaction limit.

III. IMAGE POTENTIALS OF A CHARGED PARTICLE

The image potentials can be calculated as

$$v_{\rm tot}(\mathbf{r},\omega)=\int d^3r'\,\epsilon^{-1}(\mathbf{r},\mathbf{r}',\omega)v_{\rm ext}(\mathbf{r},\omega)\,. \tag{31}$$

We consider a charge situated at z axis at a distance $z=a$,

$$v_{\rm ext}(\mathbf{r}')=\frac{Ze}{|\mathbf{r}'-\mathbf{a}|}=Ze\Phi(\mathbf{r}'-\mathbf{a})\,. \tag{32}$$

Substituting Eqs. (30) and (32) into (31), we can write

$$v_{\rm tot}(\mathbf{r})=v_{\rm ext}(\mathbf{r})+v_1(\mathbf{r})+v_2(\mathbf{r})+v_3(\mathbf{r}), \tag{33}$$

where $v_1(\mathbf{r})$, $v_2(\mathbf{r})$, and $v_3(\mathbf{r})$ correspond to the second, the third, and the terms under the summation, respectively, on the right-hand side of Eq. (30). We can define $v_1(r)$ as the on-site potential, and $v_2(\mathbf{r})$ and $v_3(\mathbf{r})$ as the interaction potentials. As our intention is to demonstrate a simple application of our model $\epsilon^{-1}(\mathbf{r},\mathbf{r}',\omega)$, we calculate $v_1(\mathbf{r})$, $v_2(\mathbf{r})$, and $v_3(\mathbf{r})$ again, neglecting the short-range interactions.

In the long-range interaction limit, $v_1(\mathbf{r})$ can be written as

$$v_1(\mathbf{r})=Zed^2\sum_{\mathbf{R}}\nabla\Phi(\mathbf{r}-\mathbf{R})\cdot\nabla\Phi(\mathbf{R}-\mathbf{a})\,. \tag{34}$$

Here, we note that, depending on the positions of field point and the charge, we get four values of Eq. (34), according to the cases (i) $|z|<d/2$ and $|a|<d/2$, (ii) $|z|<d/2$ and $|a|>d/2$, (iii) $|z|>d/2$ and $|a|<d/2$, and (iv) $|z|>d/2$ and $|a|>d/2$. Evaluating the summation over $\mathbf{R}$, we obtain, for case (i),

$$v_1(\mathbf{r})=N_0(\omega)Ze[\Phi(\mathbf{r}-\mathbf{a})-\tfrac{1}{2}\Phi_1(\mathbf{r})], \tag{35}$$

and for cases (ii)—(iv),

$$v_1(\mathbf{r})=\tfrac{1}{2}N_0(\omega)Ze\Phi_1(\mathbf{r})\alpha, \tag{36}$$

where

$$\Phi_1(\mathbf{r})=1\Big/\left[r_{||}^2+\left[\left|z-\frac{d}{2}\right|+\left|a-\frac{d}{2}\right|\right]^2\right]^{1/2}$$
$$+1\Big/\left[r_{||}^2+\left[\left|z+\frac{d}{2}\right|+\left|a+\frac{d}{2}\right|\right]^2\right]^{1/2}. \tag{37}$$

Utilizing our knowledge of the calculation of $\underline{C}\,\underline{D}_n$, $v_1(\mathbf{r})$, $v_2(\mathbf{r})$, and $v_3(\mathbf{r})$ can be calculated easily. We obtain, for case (i),

$$v_2(\mathbf{r})=Ze\alpha^2\frac{N_0^2(\omega)}{\epsilon(\omega)}[\Phi(\mathbf{r}-\mathbf{a})-\tfrac{3}{4}\Phi_1(\mathbf{r})+\tfrac{1}{4}\Phi_2(\mathbf{r})] \tag{38}$$

and

$$v_3(\mathbf{r})=\frac{Ze\alpha^2}{4}\frac{N_0^2(\omega)}{\epsilon(\omega)}\sum_{n=1}^{\infty}\left[\frac{\epsilon(\omega)-1}{\epsilon(\omega)+1}\right]^n$$
$$\times[\Phi_n(\mathbf{r})-2\Phi_{n+1}(\mathbf{r})+\Phi_{n+2}(\mathbf{r})]. \tag{39}$$

For cases (ii)—(iv), we obtain

$$v_2(\mathbf{r})=Ze\alpha^2\frac{N_0^2(\omega)}{\epsilon(\omega)}[\Phi_1(\mathbf{r})-\Phi_2(\mathbf{r})] \tag{40}$$

and

$$v_3(\mathbf{r})=\frac{Ze\alpha^2}{4}\frac{N_0^2(\omega)}{\epsilon(\omega)}\sum_{n=1}^{\infty}\left[\frac{\epsilon(\omega)-1}{\epsilon(\omega)+1}\right]^n \times[\Phi_n(\mathbf{r})-2\Phi_{n+1}(\mathbf{r})+\Phi_{n+2}(\mathbf{r})], \tag{41}$$

where

$$\Phi_n(\mathbf{r})=1/(\mathbf{r}_{||}^2+\beta_n^2)^{1/2}+1/[\mathbf{r}_{||}^2+(\beta_n')^2]^{1/2} \tag{42}$$

with

$$\beta_n=\left|z-\frac{d}{2}\right|+(n-1)d+\left|a+(-1)^n\frac{d}{2}\right| \tag{43}$$

and

$$\beta_n'=\left|z+\frac{d}{2}\right|+(n-1)d+\left|a-(-1)^2\frac{d}{2}\right| . \tag{44}$$

Combining Eqs. (33)—(44) and then summing the various series, we get, for case (i),

$$v_{\text{tot}}(\mathbf{r})=\frac{1}{\epsilon(\omega)}\left[v_{\text{ext}}(\mathbf{r})+\sum_{n=1}^{\infty}\left[\frac{\epsilon(\omega)-1}{\epsilon(\omega)+1}\right]^n\Phi_n(\mathbf{r})\right] . \tag{45}$$

For cases (ii)—(iv), we obtain

$$v_{\text{tot}}(\mathbf{r})=v_{\text{ext}}(\mathbf{r})-\sum_{n=1}^{\infty}\left[\frac{\epsilon(\omega)-1}{\epsilon(\omega)+1}\right]^n\Phi_n(\mathbf{r}) . \tag{46}$$

In Eqs. (45) and (46), the image potentials of various order appear under summation on the right-hand side. The magnitudes of these image potentials greatly depend upon the width of slab and the bulk dielectric constant $\epsilon(\omega)$. Higher-order image potentials have smaller magnitudes.

IV. DISCUSSIONS AND CONCLUSION

Equation (30) yields a model inverse dielectric response function for a semiconductor slab. The surface and finite-dimension effects emerge in terms under summation. Equation (30) includes an infinite number of image dipole terms. This shows that our model $\epsilon^{-1}(\mathbf{r},\mathbf{r}',\omega)$ contains the basic characteristics of a slab. Let us examine the two limiting cases of $\epsilon^{-1}(\mathbf{r},\mathbf{r}',\omega)$: (i) $\underline{d}$ is large and (ii) $\underline{d}$ is small. We see from Eqs. (24) and (25) that as $\underline{d}$ becomes larger and larger, the matrices $\underline{D}_1,\underline{D}_2,\underline{D}_3,\ldots,\underline{D}_n$ become smaller and smaller. This shows that as the slab becomes increasingly thicker, the finite-geometry corrections to $\epsilon^{-1}(\mathbf{r},\mathbf{r}',\omega)$ become increasingly smaller. At a very large value of $\underline{d}$, the finite-geometry effects become negligible, and Eq. (30) reduces to a bulk dielectric response function, as it should. On the other hand, as $\underline{d}$ becomes increasingly smaller, the matrices $\underline{D}_1,\underline{D}_2,\ldots,\underline{D}_n$ become increasingly larger. At very small values of $\underline{d}$, the terms under the summation completely dominate over the rest of the terms in Eq. (30). This clearly shows that in a thin slab finite-geometry effects are more important than the bulk effects. Equation (30) demonstrates how the two effects, finite-geometry and bulk effects, dominate over each other as the thickness $\underline{d}$ varies. As it was our primary aim, we have shown that like the cases of infinite or semi-infinite solids, a compact form of $\epsilon^{-1}(\mathbf{r},\mathbf{r}',\omega)$, which includes all basic characteristics of the system, can be obtained for a slab, a more complicated system with reduced symmetry. We note here that the earlier expressions of $\epsilon^{-1}(\mathbf{r},\mathbf{r}',\omega)$ for infinite and semi-infinite solids directly follow from Eq. (30) by applying the appropriate limits of $\underline{d}$.[31] Although, in obtaining $\underline{\underline{Q}}^{-1}$ we have neglected short-range interactions, Eq. (30) still contains a great deal of information about the short-range variations. The neglect of short-range interactions is not very crucial unless the slab is very thin, since the internal summations over the atomic sites go over the entire volume of slab. The short-range interactions can be included in $\underline{\underline{Q}}^{-1}$ in a perturbation approach, however, for a numerical work. As we are confined to giving the simple analytic results in this article, Eq. (3) yields a good model $\epsilon^{-1}(\mathbf{r},\mathbf{r}',\omega)$ for a slab.

As an application of our model $\epsilon^{-1}(\mathbf{r},\mathbf{r}',\omega)$, we calculated image potentials of a charged particle in the long-range interaction limit. Our results are exactly the same as those that had been obtained prior to the use of classical electrodynamics. This shows the correctness of our formulations and provides a quantum-mechanical proof of old classical results. We should note that the exact calculation of Eq. (3) provides the short-range fluctuating terms in Eqs. (45) and (46). A direct application of $v_{\text{tot}}(\mathbf{r})$ is the calculation of self-energies, which is not covered here.

As it was our primary aim, we have obtained a compact analytical form of a model RPA $\epsilon^{-1}(\mathbf{r},\mathbf{r}',\omega)$ based on a quantum-mechanical microscopic treatment. Our model $\epsilon^{-1}(\mathbf{r},\mathbf{r}',\omega)$ needs a simple integration to calculate other properties. It does not require any additional matching conditions. Extension of our calculation, in order to include short-range variations and the finite overlap in bond orbitals (band-structure effects), can be easily done using numerical methods. Also, our calculation suggests that this method can be extended to apply for composite materials, and devices having more than one junction. These topics are planned to be discussed in future publications.

ACKNOWLEDGMENTS

I would like to thank Dr. J. C. Inkson for useful discussions at the early stage of this work and Dr. M. C. Payne for useful discussions and comments on the manuscript. I acknowledge, with thanks, the financial support of the Science and Engineering Research Council (United Kingdom) at Cavendish Laboratory and the Department of Non-Conventional Energy Sources (India) at the Indian Institute of Technology, Delhi.

*Present address: Laser Technology Research Programme, Department of Physics, Indian Institute of Technology, Delhi, Hauz Khas, New Delhi-110016, India.

[1]R. Car and A. Selloni, Phys. Rev. Lett. **42**, 1365 (1979).
[2]P. M. Echnique, R. H. Ritchie, N. Barbern, and J. C. Inkson, Phys. Rev. B **23**, 6486 (1981).
[3]H. Raether, *Excitations of Plasmons and Interband Transitions* in *Springer Tracts in Modern Physics* (Springer-Verlag, Berlin, 1980), Vol. 88.
[4]W. Hanke and L. J. Sham, Phys. Rev. B **21**, 4656 (1980).
[5]W. Hanke and L. J. Sham, Phys. Rev. Lett. **33**, 582 (1974).
[6]W. Hanke, Adv. Phys. **27**, 287 (1978).
[7]K. Sturm, Adv. Phys. **31**, 1 (1982).
[8]P. E. Van Camp, V. E. Van Doren, and J. T. Devereese, Phys. Rev. Lett. **42**, 1224 (1979).
[9]Y. Onodera, Prog. Theo. Phys. **49**, 37 (1973).
[10]L. Hedin and S. Lundgvist, in *Solid State Physics: Advances in Research and Applications,* edited by F. Seitz, D. Turnbull, and H. Ehrenreich (Academic, New York, 1969), Vol. 23, p. 1.
[11]N. Wiser, Phys. Rev. **126**, 462 (1963); S. L. Adlar, *ibid.* **126**, 413 (1962).
[12]T. K. Lee and S. Kivelson, Phys. Rev. B **29**, 6687 (1984).
[13]A. Fleszar and R. Resta, Phys. Rev. B **31**, 5305 (1985).
[14]R. C. Bull and M. P. Onturo, Surf. Sci. **122**, 161 (1982).
[15]R. Bonneville, Phys. Rev. B **29**, 907 (1984).
[16]E. Fiorino and R. D. Sole, Phys. Status Solidi B **119**, 315 (1983).
[17]A. C. Sharma, J. Phys. C **18**, L153 (1985).
[18]Y. C. Lee and S. E. Ulla, J. Phys. C **17**, 2239 (1984).
[19]R. E. Camley and D. L. Mills, Phys. Rev. B **29**, 1695 (1984).
[20]A. Equiluz, T. K. Lee, J. J. Quinn, and K. W. Chiu, Phys. Rev. B **11**, 4889 (1975).
[21]H. Raether, Phys. Thin Films, **9**, 145 (1978).
[22]M. J. Rice, W. R. Schneider, and S. Strassler, Phys. Rev. B **8**, 474 (1973).
[23]A. C. Sharma and S. Auluck, J. Phys. C **15**, L1233 (1983).
[24]A. C. Sharma and S. Auluck, Phys. Lett. **96A**, 255 (1983).
[25]J. C. Inkson, J. Phys. C **7**, 1571 (1974).
[26]D. L. Price, S. K. Sinha, and R. P. Gupta, Phys. Rev. B **9**, 257 (1974).
[27]R. Resta and A. Baldereschi, Phys. Rev. B **23**, 6615 (1981).
[28]M. P. Ortuno and J. C. Inkson, J. Phys. C **12**, 1065 (1979).
[29]S. K. Sinha, R. P. Gupta, and D. L. Price, Phys. Rev. **26**, 1324 (1971).
[30]S. K. Sinha, Phys. Rev. B **177**, 1256 (1969).
[31]J. C. Inkson and A. C. Sharma, J. Phys. C **18**, 5435 (1985).